

This discussion paper is/has been under review for the journal The Cryosphere (TC).
Please refer to the corresponding final paper in TC if available.

On the substantial influence of the treatment of friction at the grounding line

O. Gagliardini^{1,2,3}, J. Brondex^{1,2}, F. Gillet-Chaulet^{1,2}, L. Tavard^{1,2}, V. Peyaud^{1,2},
and G. Durand^{1,2}

¹Univ. Grenoble Alpes, LGGE, 38041 Grenoble, France

²CNRS, LGGE, 38041 Grenoble, France

³Institut Universitaire de France, Paris, France

Received: 23 May 2015 – Accepted: 14 June 2015 – Published: 30 June 2015

Correspondence to: O. Gagliardini (olivier.gagliardini@ujf-grenoble.fr)

Published by Copernicus Publications on behalf of the European Geosciences Union.

Title Page

Abstract

Introduction

Conclusions

References

Tables

Figures

⏪

⏩

◀

▶

Back

Close

Full Screen / Esc

Printer-friendly Version

Interactive Discussion



Abstract

The dynamical contribution of marine ice sheets to sea level rise is largely controlled by grounding line (GL) dynamics. Seroussi et al. (2014) emphasised the sensitivity of numerical ice flow model results to the practical implementation of the friction of the ice on its bed in the very close vicinity of the GL. Elmer/Ice is a reference finite element (FE) ice flow model used in recent marine ice sheet model intercomparison (MISMIP) exercises. In the model, the GL is defined as the nodes where the ice is in contact with the bedrock but belong to both grounded and floating elements. Inherently to the FE method, computing the contribution of the friction by element requires evaluating the friction at the integration points. In Elmer/Ice, this is done by interpolating the values of the friction parameter C prescribed at the nodes. In this brief communication, we discuss and compare three alternative ways to prescribe the friction at the GL: (i) C is prescribed and non null at the GL nodes, (ii) C is set to zero at the GL nodes, and (iii) C is discontinuous at the GL nodes (i.e. is prescribed and non null for grounded elements and otherwise null). So far, all published results using Elmer/Ice were obtained with the first method. Using the MISMIP3d diagnostic experiment, we first show that, although the change in the total force at the base is insignificant, the three methods lead to significantly different velocity fields. We then show that these methods also lead to different steady state GL positions and different transient behaviours. Such model sensitivity to the methods discussed here is certainly specific to the high friction prescribed in the MISMIP experiments and should be smaller in real setups where friction in the vicinity of the GL would be expected to be lower. Results obtained with the three methods are available as Supplement for future comparisons.

Friction at GL in Elmer/Ice

O. Gagliardini et al.

Title Page

Abstract

Introduction

Conclusions

References

Tables

Figures



Back

Close

Full Screen / Esc

Printer-friendly Version

Interactive Discussion



1 Introduction

Marine terminating glaciers in Antarctica and Greenland control the dynamical contribution of these ice sheets to sea level rise. Among the processes at play, the retreat of the grounding line (GL) has a major impact on this dynamical contribution. Accurate modelling of GL dynamics is therefore a precondition for prognostic simulations of the future of ice sheets in a warming climate. Previous works have emphasised the importance of the mesh resolution around the GL (Vieli and Payne, 2005; Durand et al., 2009a, b; Pattyn et al., 2012) and how the friction is interpolated in the vicinity of the GL (Gladstone et al., 2012; Seroussi et al., 2014; Leguy et al., 2014). Two recent intercomparison exercises were designed to compare and test the ability of ice-sheet models to resolve the advance and retreat of the GL based on different perturbations. MIS-MIP was dedicated to two-dimensional flow line geometry (Pattyn et al., 2012) and used an analytical solution (Schoof, 2007), whereas MIS-MIP3d was a fully three-dimensional setup (Pattyn et al., 2013).

Elmer/Ice was the only Stokes model to perform the MIS-MIP experiment 3a (Pattyn et al., 2012) and it was one of only two Stokes models to perform the whole MIS-MIP3d experiments (Pattyn et al., 2013). Moreover, in the latter intercomparison exercise, the diagnostic experiment P75D was directly build from the geometry obtained with Elmer/Ice after the 100 year perturbation experiment. As the only Stokes model to perform the two intercomparison exercises, Elmer/Ice results are currently used as references for comparison with other models based on lower order Stokes equations. The results of the MIS-MIP and MIS-MIP3d intercomparisons obtained with Elmer/Ice have also been used as benchmarks to test Stokes models during their development.

Using a finite element lower order Stokes model (Shallow Shelf Approximation, SSA), Seroussi et al. (2014) compared various parameterisations of the GL position. Using the SSA, the GL position is directly evaluated from the floatation criterion and can therefore be located at any point of the domain and not only at the element nodes. In this way, the basal friction can be evaluated with a subgrid resolution. Their results

TCD

9, 3475–3501, 2015

Friction at GL in Elmer/Ice

O. Gagliardini et al.

Title Page

Abstract

Introduction

Conclusions

References

Tables

Figures



Back

Close

Full Screen / Esc

Printer-friendly Version

Interactive Discussion



revealed the high sensitivity of the GL dynamics to the treatment of basal friction in the close vicinity of the GL and also showed that sub-element parametrisation of the GL significantly reduces the sensitivity of the results to the mesh size at the GL.

Unfortunately, for the Stokes problem, sub-element parametrisation cannot be applied to solve the contact between the ice and its bed. Indeed, the contact condition can only be evaluated at the element nodes. Therefore, the only way to improve the accuracy of the model is to increase the mesh refinement in the close vicinity of the GL (Durand et al., 2009b). However, even if a sub-element parameterisation of the GL cannot be used, there is more than one possible way of treating the friction in the vicinity of the GL.

The aim of this paper is to present three possible ways to apply friction at the GL and the resulting differences in terms of GL dynamics. First we present the three methods and their specificities. Then, using MISMIP and MISMIP3d setups, we compare the three methods in advance and retreat configurations of the GL.

2 Friction in the close vicinity of the GL

Elmer/Ice uses the finite element method and, by construction, all the field variables are defined as nodal values and so is the GL which follows the edges of the elements. The GL dynamics is solved as a contact problem between the ice and the underlying bed. The effectiveness of the contact is tested for each node belonging on the bed by comparing the residual force of the Stokes equations to the force exerted by the sea water pressure (for more details, see Durand et al., 2009a). By definition, the GL is the ensemble of nodes which are the last in contact with the bedrock, i.e. for which the Stokes residual is strictly larger than the water force. Furthermore, the GL marks the transition between ice in contact with the bedrock, and therefore subject to friction, and ice in contact with the ocean with a free slip condition.

Three modelling strategies can be used to impose this transition at the GL between the slip condition to the free-slip condition (see Fig. 1). The first strategy is assuming

Friction at GL in Elmer/Ice

O. Gagliardini et al.

Title Page

Abstract

Introduction

Conclusions

References

Tables

Figures



Back

Close

Full Screen / Esc

Printer-friendly Version

Interactive Discussion



Friction at GL in Elmer/Ice

O. Gagliardini et al.

Title Page

Abstract

Introduction

Conclusions

References

Tables

Figures



Back

Close

Full Screen / Esc

Printer-friendly Version

Interactive Discussion



that the GL defines the last grounded (LG) nodes and that friction is applied up to the nodes belonging to the GL. In the second, the nodes belonging to the GL are assumed to be the first floating (FF) nodes and are already freely slipping. The third strategy assumes that the friction is discontinuous (DI) at the nodes belonging to the GL: friction at these nodes is only applied if integrating over an element where all other nodes are also in contact with the bedrock but a free slip condition is applied if the node belongs to an element where at least one node is in contact with the ocean. The three methods are illustrated in a two-dimensional flow line configuration in Fig. 1.

To build the finite element system to be solved, the friction needs to be interpolated at the integration points of each element. For the LG method, the first elements in contact with the ocean are therefore undergoing some friction due to the interpolation between a non-zero friction value at the nodes belonging to the GL and zero value at the other nodes. On the contrary, for the FF method the friction is lowered in the last elements in contact with the bedrock because of the vanishing friction at the GL nodes. The DI method is therefore certainly the most physical as friction is applied up to the GL but switched off in the first elements in contact with ocean. However the three methods should converge to the same solution when the elements size decreases. Moreover, the three methods should give identical results if the friction at the GL is null, whatever the mesh discretisation. Up to now, all the published Elmer/Ice results were obtained using the LG method (Durand et al., 2009a, b, 2011; Gagliardini et al., 2010, 2013; Favier et al., 2012, 2014; Drouet et al., 2013; Gudmundsson et al., 2012; Pattyn et al., 2012, 2013; Krug et al., 2014). In the following sections, we compare the three methods using numerical experiments proposed in MISMIP and MISMIP3d, known to present high contrast in friction at the GL. Doing so, the obtained differences between the three methods presented in this paper might be seen as upper bound values for more realistic cases with a smooth transition in friction at the GL.

3 Influence on the flux at the GL

The three methods are first compared using the diagnostic experiment P75D of MIS-MIP3d. The objective of experiment P75D was to compare the velocity field obtained by the various Stokes approximations for a prescribed glacier geometry. This geometry, the same for all numerical models, was defined as the one obtained with Elmer/Ice at $t = 100$ a for experiment P75S (the last time step of the perturbation experiment, see below and Pattyn et al. (2013) for more details on the experimental setups). We recall that at that time this geometry was obtained using the LG method. Exactly the same mesh as in Pattyn et al. (2013) is used here to compare the three methods on this diagnostic experiment.

In Pattyn et al. (2013), the boundary condition (BC) applied at the base of the ice-shelf for the diagnostic experiment was not specified. If this condition is clear for lower-order Stokes models (i.e. for vertically integrated models), this is not the case when solving for the full-Stokes solution. In the next part, the possible BCs to be applied at the base of the ice-shelf are presented. The velocity field obtained with the three methods for interpolating the friction at the GL are then compared.

3.1 BC below ice-shelf for a diagnostic simulation

In this part we give more details about the different possibilities for the BC at the base of the ice-shelf. Which BC to be applied was not specified for the diagnostic experiment in Pattyn et al. (2013). For a Stokes *prognostic* simulation, assuming no accretion/melting, Durand et al. (2009a) have shown that the following BC should be applied at the base of the ice-shelf:

$$\sigma_{nn}|_b = -\rho_w g (l_w - z_b) + C_n u_n, \quad (1)$$

where l_w and z_b are the sea and ice-shelf bottom elevations, respectively, ρ_w the water density, g the gravity, $u_n = \mathbf{u} \cdot \mathbf{n}$ the normal component of the ice velocity and

$C_n = \rho_w g \sqrt{1 + (\partial z_b / \partial x)^2 + (\partial z_b / \partial y)^2} dt$. As explained in Durand et al. (2009a), C_n

TCD

9, 3475–3501, 2015

Friction at GL in
Elmer/Ice

O. Gagliardini et al.

Title Page

Abstract

Introduction

Conclusions

References

Tables

Figures

◀

▶

◀

▶

Back

Close

Full Screen / Esc

Printer-friendly Version

Interactive Discussion



acts like a damper on the bottom interface so that the normal stress induced by $C_n u_n$ will counteract the buoyancy stress and will avoid too large velocity that would arise even for a small buoyancy disequilibrium.

For a Stokes *diagnostic* simulation, one can think about two other BC for the ocean/ice interface. For all of them we implicitly assume that there is no melting or marine ice accretion below the ice-shelf. The first, a Dirichlet BC, sets that the velocity normal to the bottom surface is null, i.e.

$$u_n = \mathbf{u} \cdot \mathbf{n} = 0. \quad (2)$$

The second, a Neumann BC, assumes the buoyancy equilibrium at the interface ice/ocean:

$$\sigma_{nn}|_b = -\rho_w g (l_w - z_b). \quad (3)$$

Equation (1) derives from Eq. (3) with an implicit evaluation of z_b at $t + dt$ using the free surface equation for z_b .

For a steady-state geometry, all three BC should give the same velocity field as one expects $u_n = 0$ and the buoyancy equilibrium to be fulfilled. Here, for the diagnostic experiment P75D, because the geometry does correspond to a snapshot of a transient evolution, the ice-shelf is not exactly at the buoyancy equilibrium. This is true for the LG method with which the geometry was obtained, and even worse for the two other methods which have completely different geometries after the 100 year perturbation (see discussion below and Fig. 6). We therefore tested the three possibilities for the bottom ice-shelf BC.

Even for the LG method, no convergence of the non-linear iteration was obtained with the Neumann BC (Eq. 3). This indicates that even a small buoyancy disequilibrium renders the Stokes problem ill-posed. Adding the viscous damper C_n to the hydrostatic stress (BC given by Eq. 1) has a stabilisation effect and allow convergence. No results are therefore presented for the BC (Eq. 3). Results for the two other BCs are presented in the next part.

Friction at GL in Elmer/Ice

O. Gagliardini et al.

Title Page

Abstract

Introduction

Conclusions

References

Tables

Figures

⏪

⏩

◀

▶

Back

Close

Full Screen / Esc

Printer-friendly Version

Interactive Discussion



3.2 Results from MISMIP3d P75D

Changes along the x direction of the x component of the surface velocity at $y = 0$ (symmetry axis for the flow and centre for the perturbation of the basal friction parameter) and at $y = 50$ km (side of the domain) are presented for all three methods and for the two BCs (Eq. 1) and Eq. (2) in Fig. 2. As can be seen in this figure, the LG method leads to the smallest velocity and the FF method to the largest, while the velocity obtained with the DI method is between the two. The way the friction is interpolated at the GL not only influences the velocity downstream from the GL but also over a few ice thicknesses upstream from the GL. At the GL, the relative difference in velocity between LG and FF methods is as high as 23% for $y = 0$ and 17% for $y = 50$ km. The difference is greater at $y = 0$ than at $y = 50$ km despite less friction at the GL at $y = 0$ than at $y = 50$ km. As the vertical gradients of horizontal velocity are small at the GL, similar differences would be expected in ice fluxes through the GL. Such differences are very large in comparison to the differences in the total basal traction between the three methods. The relative difference between LG and FF methods of the tangential stress integrated over the bed was found to be $\approx 10^{-5}$, at least 4 orders of magnitude less than the difference obtained for velocity. Despite an insignificant change in the total force at the base, the way the friction law is applied in the very close vicinity of the GL is found to have a significant effect on the velocity field.

The Elmer/Ice velocity solution for experiment P75D in Pattyn et al. (2013) is also shown in Fig. 2 (black curve, named LFA in Pattyn et al., 2013). As Elmer/Ice has been used to design the experiment, the geometry and velocity field were directly extracted from the last time step of the transient experiment P75S. Because of the time-integration scheme in Elmer/Ice, the velocity field was in fact computed from the previous time step geometry ($t - 0.5$ a), and not computed as the steady-state solution of the geometry provided. This explains the minor difference between the published velocity solution and the newly computed LG solution (brown thick curve in Fig. 2).

TCO

9, 3475–3501, 2015

Friction at GL in Elmer/Ice

O. Gagliardini et al.

Title Page

Abstract

Introduction

Conclusions

References

Tables

Figures



Back

Close

Full Screen / Esc

Printer-friendly Version

Interactive Discussion



Friction at GL in Elmer/Ice

O. Gagliardini et al.

Title Page

Abstract

Introduction

Conclusions

References

Tables

Figures



Back

Close

Full Screen / Esc

Printer-friendly Version

Interactive Discussion



The two solutions for the BC below the ice-shelf give slightly different results for all three methods. As shown in Fig. 2, the horizontal flow at the GL for BC (Eq. 2) is found to be slower by approximately 1 % than the one for BC (Eq. 1), for all three methods and both at $y = 0$ and $y = 50$ km. For BC (Eq. 1), despite its theoretical validity only for transient simulation (time step dt entering Eq. 1), the results presented in Fig. 2 were obtained assuming an arbitrary time step $dt = 1$ a. Anyway, other realistic choices of dt would not change significantly the results as the term $C_n u_n$ in Eq. (1) is found to be at least 10^3 times smaller than the hydrostatic pressure $-\rho_w g(l_w - z_b)$. Because the Dirichlet boundary condition (Eq. 2) is certainly the easiest to implement and test, the results for both BCs (Eqs. 1 and 2) are given as Supplement. For future comparisons, it would be therefore more consistent to use the results in the Supplement of the present publication, either with the buoyancy BC (Eq. 1) or the Dirichlet BC (Eq. 2) applied at the base of the ice-shelf.

For this diagnostic application, the influence of the mesh discretisation has not been inferred. Nevertheless, as expected theoretically, and as will be shown in the following part, the difference between the three methods should decrease by increasing the mesh refinement in the vicinity of the GL.

4 Influence on the GL dynamics

The previous part has indicated a strong sensitivity of the velocity field to the chosen method to interpolate the friction at the GL, and one might therefore expect similar sensitivity on the GL steady state position and GL dynamics. To study this sensitivity, the three methods are compared using both MISMIP and MISMIP3d experiments.

4.1 MISMIP 3a like experiments

This part presents results on the sensitivity to the mesh resolution using a flow line configuration. For that purpose, the GL dynamics is studied using a set up adapted

Friction at GL in
Elmer/Ice

O. Gagliardini et al.

Title Page

Abstract

Introduction

Conclusions

References

Tables

Figures



Back

Close

Full Screen / Esc

Printer-friendly Version

Interactive Discussion



from experiment 3a of the MISIMP intercomparison exercise (Pattyn et al., 2012). Experiment 3a assumes an overdeepened bedrock, a non-linear Weertman friction law and that the GL is evolved by step changes of the ice fluidity parameter. Previous works have shown that steady-state position of GL could differ slightly depending on whether it is obtained from advancing or retreating GL, but that this difference decreased with an increase in mesh resolution (Durand et al., 2009a). We will therefore compare the three methods in cases of both advance and retreat and with various mesh discretizations. Starting from the ice-sheet geometry given by the semi-analytical solution of Schoof (2007) for steps 1 and step 5 of experiment 3a (see Pattyn et al. (2012) for more details), the ice fluidity for step 3 is then applied and the geometry is evolved until a steady state is obtained, one in advance (from step 1 to step 3) and one in retreat (from step 5 to step 3).

Results are presented in Fig. 3 and in Table 1. These results were obtained using the same type of mesh than the one used for producing the Elmer/Ice MISIMP results, with an evolving resolution along the flow direction (see Durand et al. (2009a) for more details). For all configurations, the LG method leads to the most advanced GL, the FF method to the least advanced GL and the DI method to an intermediate GL position. For a given discretisation, differences on the steady GL position from the three methods are of the same order than differences from advance to retreat (comparison of Fig. 3b and c). For a 200 m discretization, the difference between the LG and FF methods is 18.2 km in advance and 21 km in retreat. The DI position is almost exactly half way between the LG and FF positions. With a 25 m resolution at the GL, these differences are reduced to less than 2 km in both advance and retreat. For the purpose of comparison, with a given method, the difference between advance and retreat is around ≈ 26 km at the resolution of 200 m and is decreased to less than 3 km at a resolution of 25 m.

Figure 3a also shows the published Elmer/Ice GL position obtained in advance from step 2 to step 3 in Pattyn et al. (2012). This solution was produced using the same discretisation of 200 m at the GL, but not exactly the same mesh. Despite the same discretisation at the GL, there is a 3 km difference with the new LG solution. In line

with Durand et al. (2009b), these differences illustrate the sensitivity of the GL position not only to the mesh resolution at the GL, but also to the other mesh characteristics, and more specifically how strongly the mesh resolution is reduced downstream and upstream the GL.

In the previous analysis, we only focussed on the final steady state position of the GL. Using the same experiments, we accessed the transient response by plotting the GL position as well as the rate of change in the volume above floatation (VAF), as a function of time (see Figs. 4 and 5). Because the initial geometries are the same for the three methods (step 1 and step 5 given by Schoof, 2007), but the steady state solutions are different, it appears that the rate of change of the VAF is mainly controlled by the distance from the steady solution. In other words, the longer the distance between the initial geometry and the steady state, the higher the rate of change of the VAF. For the 25 m resolution, the different steady state geometries being very close, VAF rate of changes are also very similar.

As expected theoretically, the MISMIP flow line study confirms that, despite a high jump in friction at the GL, all three methods converge to an identical solution as the mesh resolution is improved, but can lead to significantly different solutions for a too coarse mesh.

4.2 MISMIP3d P75S and P75R

The three methods are finally compared using the prognostic experiments of MISMIP3d. This experiment is decomposed in three steps. First, assuming no lateral variation in y , a steady state geometry is obtained for each model. In the second step, P75S, a Gaussian sliding perturbation is introduced precisely at the grounding line and centred on the axis of symmetry at $y = 0$ km. This constant perturbation is applied for the next 100 years. Finally, during the last step, P75R, the perturbation is removed and the GL moves back to its initial steady position. Only the first 100 years of the removal are studied. Note that for the grounding line to get back to its initial steady state position

Friction at GL in Elmer/Ice

O. Gagliardini et al.

Title Page

Abstract

Introduction

Conclusions

References

Tables

Figures



Back

Close

Full Screen / Esc

Printer-friendly Version

Interactive Discussion



might take much longer than 100 years as the behaviour in advance and retreat is not symmetrical.

The three methods are first compared using a mesh with similar discretisations in both longitudinal and lateral directions as the one used to obtain the LFA results in Pattyn et al. (2013). Because the steady state geometries are different for the three methods, all meshes present similar features (same number of nodes, same refinement at the GL) but cannot be identical.

As expected from the results presented in the previous part, the steady GL positions obtained with the three methods are significantly different, the LG solution being more advanced by ≈ 7 km in comparison to the FF one (see Table 2). It should be noticed that this distance is similar to the one obtained between the LG solution and the LFA solution published in Pattyn et al. (2013), using the same discretisation at the GL but not exactly the same mesh. This gives an indication on how the results are sensitive to the mesh, and not only in the vicinity of the GL. In what follows, the transient response is discussed relative to the steady GL position x_{G_0} of each model.

Figure 6 shows the evolution of the GL during the 100 years of the perturbation and during the same time after the perturbation has been removed, at $y = 0$ and $y = 50$ km. As shown in this figure, the transient responses of the three methods relative to their initial position x_{G_0} are similar during the first 5 years, but then differ significantly. Interestingly, if the LG GL is continuously advancing at $y = 0$, this is not anymore the case for the two other methods. The rapid advance of the FF GL position at $y = 0$ occurring during the first years is then followed by a retreat of almost the same magnitude after 100 years, with a difference lower than 2 km with the initial GL position, when it is almost 19 km for the LG one (see Table 2). After the perturbation is removed, the GL starts to move back towards its initial steady state position. Nevertheless, after 100 years (dashed lines from 100 to 0 a in Fig. 6), the GLs are still far from having reached again the steady state position ($\Delta_{x_G} = 0$). The LG method is the fastest in coming back to its steady state position whereas the FF is the slowest.

Friction at GL in Elmer/Ice

O. Gagliardini et al.

Title Page

Abstract

Introduction

Conclusions

References

Tables

Figures



Back

Close

Full Screen / Esc

Printer-friendly Version

Interactive Discussion



Friction at GL in Elmer/Ice

O. Gagliardini et al.

Title Page

Abstract

Introduction

Conclusions

References

Tables

Figures



Back

Close

Full Screen / Esc

Printer-friendly Version

Interactive Discussion



Such large differences for the transient response of the three methods can only be explained by a too coarse mesh. The steady solution being reasonably close, and independent of the lateral discretisation of the mesh (no transverse variation of any field so that the steady GL is a straight line perpendicular to the x direction), the source of discrepancy for the transient response certainly arises from the lateral discretisation. The number of lateral elements N_y is only 20 for the previous simulations. The sensitivity of the transient response to the lateral discretisation is investigated by running the same experiment with two finer lateral mesh resolution, everything else being the same. Results for $N_y = 40$ and $N_y = 80$ are presented in Figs. 7 and 8, respectively. As can be seen by comparing Figs. 6–8 (see also Table 2), differences in the transient response of the three methods are significantly decreased when the lateral mesh refinement is increased. Nevertheless, even with the finer mesh ($N_y = 80$), the difference between the methods stays relatively important (≈ 5 km between LG and FF at the end of the perturbation experiment, but to be compared to 17 km for $N_y = 20$). Higher lateral discretisation were not further explored for computing resource purpose, but this study clearly indicates that, as expected theoretically and shown in the previous part using the flow line setup MISMIP, the difference between the three methods is decreased as the mesh resolution is increased. Published LFA results (Pattyn et al., 2013) were obtained with a lateral discretisation of $N_y = 20$ elements, which was certainly insufficient as shown by these new results using 40 and 80 lateral elements. For further comparisons, we recommend to use the more accurate results presented in Fig. 8 and provided as Supplement.

5 Conclusions

In this paper, we have presented three methods for the treatment of the friction at the GL for a finite element formulation of the Stokes equations. So far, in all the applications using Elmer/Ice, it was assumed that the friction is applied up to the GL using the LG

method. In so doing, the first elements immediately downstream from the GL undergo a little friction even if being in contact with the ocean.

We have shown that despite its very limited influence on the total force balance, the treatment of the friction at the GL has a major influence on both the velocity field and on the resulting GL dynamics. As expected theoretically, the difference between the three methods is shown to decrease as the mesh resolution is increased. Nevertheless, even for the smallest refinements accessed for the three-dimensional test case, significant differences are still observed. This give an indication on the model error to be expected when performing GL dynamics simulations. Moreover, using MISMIP3d experiment, the lateral refinement is shown to have also a significant influence on the transient behaviour. All these results were obtained using the MISMIP and MISMIP3d setups, which are known to present a very high friction at the GL.

Because the GL is in contact with the ocean, one would expect basal friction to vanish at the GL, i.e. that the friction parameter C tends to zero as the upstream distance to the GL tends to zero. In such a case, if $C = 0$ at the GL, it is clear that all three methods (LG, DI and FF) would be identical and therefore result in the same solution whatever the mesh resolution. Consequently, we expect that for more realistic applications, the sensitivity of the model results to the choice of the friction treatment at the GL would be smaller. The methods proposed by Pattyn et al. (2006), Leguy et al. (2014), Tsai et al. (2015) and Gladstone et al. (2015) present interesting approaches in that direction. Future intercomparison exercises should adopt such approaches to avoid too large jump in friction at the GL and allow the comparison of the different models on more realistic setups. In any case, we recommend to use the discontinuous DI method which is certainly the most realistic of the three. We also recommend to use these newly published results for model comparison.

**The Supplement related to this article is available online at
doi:10.5194/tcd-9-3475-2015-supplement.**

Friction at GL in Elmer/Ice

O. Gagliardini et al.

Title Page

Abstract Introduction

Conclusions References

Tables Figures

⏪ ⏩

◀ ▶

Back Close

Full Screen / Esc

Printer-friendly Version

Interactive Discussion



Acknowledgements. This study was funded by the Agence Nationale pour la Recherche (ANR) through the SUMER, Blanc SIMI 6-2012. The new simulations presented in this paper have been done using the high-performance computing resources of CINES (Centre Informatique National de l'Enseignement Supérieur, France) under allocations 2015-016066 made by GENCI (Grand Equipement National de Calcul Intensif).

References

- Drouet, A. S., Docquier, D., Durand, G., Hindmarsh, R., Pattyn, F., Gagliardini, O., and Zwinger, T.: Grounding line transient response in marine ice sheet models, *The Cryosphere*, 7, 395–406, doi:10.5194/tc-7-395-2013, 2013. 3479
- Durand, G., Gagliardini, O., de Fleurian, B., Zwinger, T., and Le Meur, E.: Marine ice sheet dynamics: hysteresis and neutral equilibrium, *J. Geophys. Res.-Earth*, 114, F03009, doi:10.1029/2008JF001170, 2009a. 3477, 3478, 3479, 3480, 3484
- Durand, G., Gagliardini, O., Zwinger, T., Le Meur, E., and Hindmarsh, R. C. A.: Full-Stokes modeling of marine ice-sheets: influence of the grid size, *Ann. Glaciol.*, 52, 109–114, doi:10.3189/172756409789624283, 2009b. 3477, 3478, 3479, 3485
- Durand, G., Gagliardini, O., Favier, L., Zwinger, T., and Le Meur, E.: Impact of bedrock description on modeling ice sheet dynamics, *Geophys. Res. Lett.*, 38, L20501, doi:10.1029/2011GL048892, 2011. 3479
- Favier, L., Gagliardini, O., Durand, G., and Zwinger, T.: A three-dimensional full Stokes model of the grounding line dynamics: effect of a pinning point beneath the ice shelf, *The Cryosphere*, 6, 101–112, doi:10.5194/tc-6-101-2012, 2012. 3479
- Favier, L., Durand, G., Cornford, S., Gudmundsson, G., Gagliardini, O., Gillet-Chaulet, F., Zwinger, T., Payne, A., and Le Brocq, A.: Retreat of Pine Island Glacier controlled by marine ice-sheet instability, *Nat. Clim. Change*, 4, 117–121, doi:10.1038/nclimate209, 2014. 3479
- Gagliardini, O., Durand, G., Zwinger, T., Hindmarsh, R., and Le Meur, E.: Coupling of ice-shelf melting and buttressing is a key process in ice-sheets dynamics, *Geophys. Res. Lett.*, 37, L14501, doi:10.1029/2010GL043334, 2010. 3479
- Gagliardini, O., Zwinger, T., Gillet-Chaulet, F., Durand, G., Favier, L., de Fleurian, B., Greve, R., Malinen, M., Martín, C., Råback, P., Ruokolainen, J., Sacchetti, M., Schäfer, M., Seddik, H.,

TCO

9, 3475–3501, 2015

Friction at GL in Elmer/Ice

O. Gagliardini et al.

Title Page

Abstract

Introduction

Conclusions

References

Tables

Figures

◀

▶

◀

▶

Back

Close

Full Screen / Esc

Printer-friendly Version

Interactive Discussion



Friction at GL in
Elmer/Ice

O. Gagliardini et al.

Title Page

Abstract

Introduction

Conclusions

References

Tables

Figures

I ◀

▶ I

◀

▶

Back

Close

Full Screen / Esc

Printer-friendly Version

Interactive Discussion



and Thies, J.: Capabilities and performance of Elmer/Ice, a new-generation ice sheet model, *Geosci. Model Dev.*, 6, 1299–1318, doi:10.5194/gmd-6-1299-2013, 2013. 3479

Gladstone, R. M., Lee, V., Rougier, J., Payne, A. J., Hellmer, H., Le Brocq, A., Shepherd, A., Edwards, T. L., Gregory, J., and Cornford, S. L.: Calibrated prediction of Pine Island glacier retreat during the 21st and 22nd centuries with a coupled flowline model, *Earth Planet. Sc. Lett.*, 333, 191–199, 2012. 3477

Gladstone, R. M., Warner, R., Budd, W., Galton-Fenzi, B., Gagliardini, O., Zwinger, T., and Greve, R.: Marine ice sheet model performance depends on basal sliding physics and sub-shelf melting, *The Cryosphere*, in preparation, 2015. 3488

Gudmundsson, G. H., Krug, J., Durand, G., Favier, L., and Gagliardini, O.: The stability of grounding lines on retrograde slopes, *The Cryosphere*, 6, 1497–1505, doi:10.5194/tc-6-1497-2012, 2012. 3479

Krug, J., Weiss, J., Gagliardini, O., and Durand, G.: Combining damage and fracture mechanics to model calving, *The Cryosphere*, 8, 2101–2117, doi:10.5194/tc-8-2101-2014, 2014. 3479

Leguy, G. R., Asay-Davis, X. S., and Lipscomb, W. H.: Parameterization of basal friction near grounding lines in a one-dimensional ice sheet model, *The Cryosphere*, 8, 1239–1259, doi:10.5194/tc-8-1239-2014, 2014. 3477, 3488

Pattyn, F., Huyghe, A., De Brabander, S., and De Smedt, B.: Role of transition zones in marine ice sheet dynamics, *J. Geophys. Res.*, 111, F02004, doi:10.1029/2005JF000394, 2006. 3488

Pattyn, F., Schoof, C., Perichon, L., Hindmarsh, R. C. A., Bueler, E., de Fleurian, B., Durand, G., Gagliardini, O., Gladstone, R., Goldberg, D., Gudmundsson, G. H., Huybrechts, P., Lee, V., Nick, F. M., Payne, A. J., Pollard, D., Rybak, O., Saito, F., and Vieli, A.: Results of the Marine Ice Sheet Model Intercomparison Project, MISIP, *The Cryosphere*, 6, 573–588, doi:10.5194/tc-6-573-2012, 2012. 3477, 3479, 3484, 3496

Pattyn, F., Perichon, L., Durand, G., L., F., Gagliardini, O., Hindmarsh, R. C. A., Zwinger, T., Albrecht, T., Cornford, S., Docquier, D., Fürst, J. J., Golberg, D., Gudmundsson, G. H., Humbert, A., Hütten, M., Huybrechts, P., Jouvét, G., Kleiner, T., Larour, E., Martin, D., Morlighem, M., Payne, A. J., Pollard, D., Rückamp, M., Rybak, O., Seroussi, H., Thoma, M., and Wilkens, N.: Grounding-line migration in plan-view marine ice-sheet models: results of the ice2sea MISIP3d intercomparison, *J. Glaciol.*, 59, 410–422, doi:10.3189/2013JoG12J129, 2013. 3477, 3479, 3480, 3482, 3486, 3487, 3493, 3495, 3499

- Schoof, C.: Ice sheet grounding line dynamics: steady states, stability, and hysteresis, *J. Geophys. Res.*, 112, F03S28, doi:10.1029/2006JF000664, 2007. 3477, 3484, 3485, 3496
- Seroussi, H., Morlighem, M., Larour, E., Rignot, E., and Khazendar, A.: Hydrostatic grounding line parameterization in ice sheet models, *The Cryosphere*, 8, 2075–2087, doi:10.5194/tc-8-2075-2014, 2014. 3476, 3477
- 5 Tsai, V. C., Stewart, A. L., and Thompson, A. F.: Marine ice-sheet profiles and stability under Coulomb basal conditions, *J. Glaciol.*, 61, 205–215, 2015. 3488
- Vieli, A. and Payne, A.: Assessing the ability of numerical ice sheet models to simulate grounding line migration, *J. Geophys. Res.*, 110, F01003, doi:10.1029/2004JF000202, 2005. 3477

Friction at GL in Elmer/Ice

O. Gagliardini et al.

Title Page

Abstract

Introduction

Conclusions

References

Tables

Figures



Back

Close

Full Screen / Esc

Printer-friendly Version

Interactive Discussion



Friction at GL in Elmer/Ice

O. Gagliardini et al.

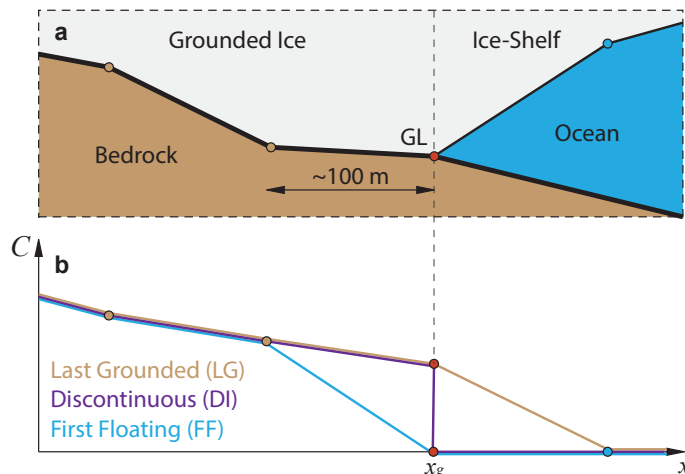


Figure 1. Two-dimensional schematic explanation of the three different alternatives to impose the friction in the close vicinity of the GL. **(a)** Zoom on the triple junction point between ice, bedrock and ocean, defined as the GL (red dot and x_g) and **(b)** changes in the friction parameter C close to the GL, with the three methods: friction is applied at the GL which is then the last grounded node (LG, brown), pure sliding is applied at the GL which is then the first floating node (FF, blue) and the friction is discontinuous at the GL (DI, purple). The coloured dots are the bottom boundary nodes of the finite element mesh: brown in contact with the bedrock, blue in contact with the ocean and red at the GL.

[Title Page](#)
[Abstract](#)
[Introduction](#)
[Conclusions](#)
[References](#)
[Tables](#)
[Figures](#)
[◀](#)
[▶](#)
[◀](#)
[▶](#)
[Back](#)
[Close](#)
[Full Screen / Esc](#)
[Printer-friendly Version](#)
[Interactive Discussion](#)


Friction at GL in Elmer/Ice

O. Gagliardini et al.

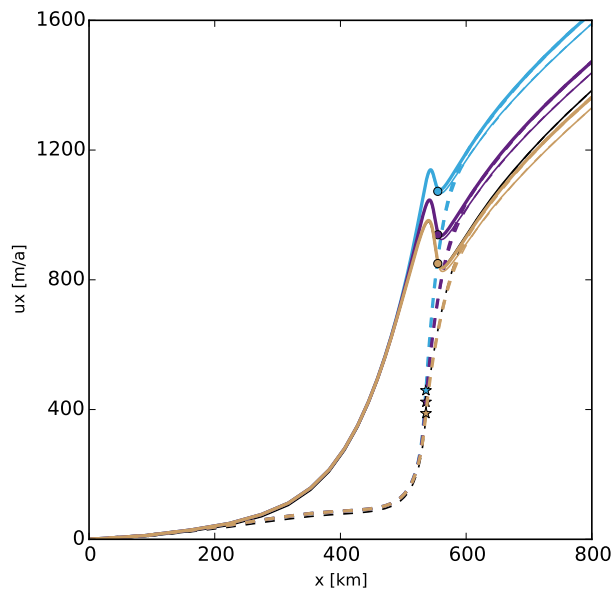


Figure 2. Experiment MISMIP3d P75D: surface velocity along the x direction for the three different methods: LG (brown), DI (purple) and FF (blue) on the symmetry axis ($y = 0$; continuous line) and on the free-slip boundary ($y = 50$ km, dashed line), for BC (Eq. 1) (thick line) and BC (Eq. 2) (thin line). The LFA Elmer/Ice solution published in Pattyn et al. (2013) is represented in black (mostly hidden by the LG brown thick curve). The signs indicate the GL position in $y = 0$ (dot) and $y = 50$ km (star).

Title Page

Abstract

Introduction

Conclusions

References

Tables

Figures

◀

▶

◀

▶

Back

Close

Full Screen / Esc

Printer-friendly Version

Interactive Discussion



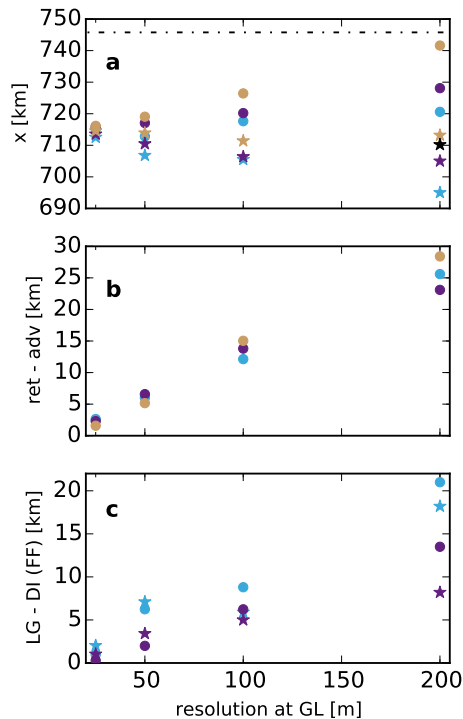


Figure 3. Experiment MISMP 3a step 3: **(a)** grounding line positions in advance (stars) and retreat (dots) obtained with the three different methods LG (brown), DI (purple) and FF (blue), **(b)** difference in the position of GL in advance and retreat obtained with the three different methods (same colour legend), and **(c)** difference between the LG solutions and the two others, as a function of mesh resolution at the GL. In **(a)**, the black star corresponds to the published GL position for step 3 of experience 3a in Pattyn et al. (2012) and the dot-dashed line is the Schoof (2007) solution.

Friction at GL in Elmer/Ice

O. Gagliardini et al.

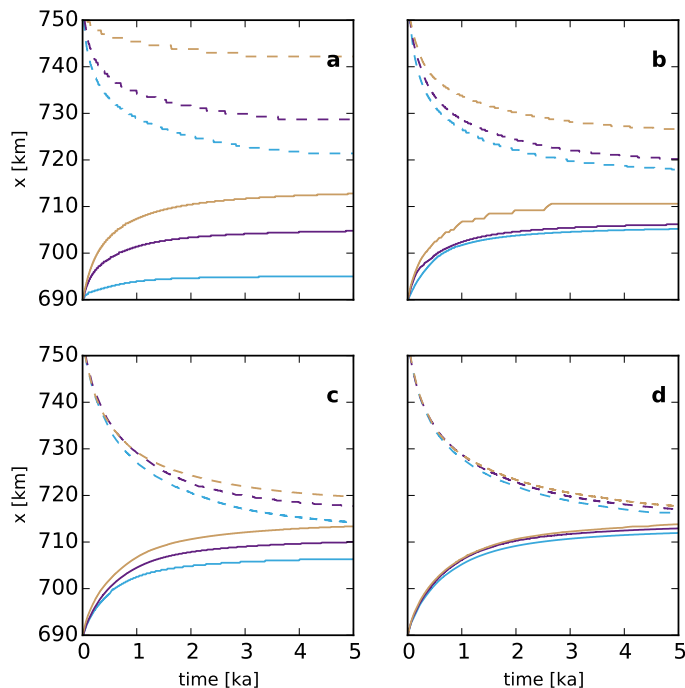


Figure 4. Experiment MISMIP 3a, steps 1 to 3 (advance) and 5 to 3 (retreat): evolution with time of the GL position for the three methods LG (brown), DI (purple) and FF (blue) in advance (solid line) and in retreat (dashed line) for the four resolutions **(a)** 200 m, **(b)** 100 m, **(c)** 50 m and **(d)** 25 m. The steady state GL positions plotted in Fig. 3 and given in Table 1 are obtained at $t = 10$ ka. This figure focusses on the first 5 ka.

Title Page

Abstract

Introduction

Conclusions

References

Tables

Figures

I ◀

▶ I

◀

▶

Back

Close

Full Screen / Esc

Printer-friendly Version

Interactive Discussion



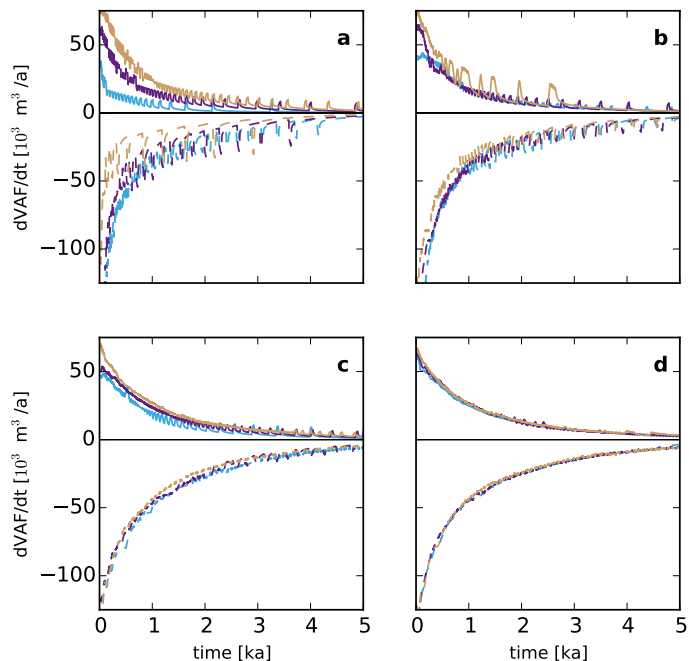


Figure 5. Experiment MISMIP 3a, steps 1 to 3 (advance) and 5 to 3 (retreat): evolution with time of the rate of change of the VAF for the three methods LG (brown), DI (purple) and FF (blue) in advance (solid line) and in retreat (dashed line) for the four resolutions **(a)** 200 m, **(b)** 100 m, **(c)** 50 m and **(d)** 25 m. The rate of change of the VAF is averaged over a 20 year time window. The steady state GL positions plotted in Fig. 3 and given in Table 1 are obtained at $t = 10$ ka. This figure focusses on the first 5 ka.

[Title Page](#)
[Abstract](#)
[Introduction](#)
[Conclusions](#)
[References](#)
[Tables](#)
[Figures](#)
[I ◀](#)
[▶ I](#)
[◀](#)
[▶](#)
[Back](#)
[Close](#)
[Full Screen / Esc](#)
[Printer-friendly Version](#)
[Interactive Discussion](#)


Friction at GL in Elmer/Ice

O. Gagliardini et al.

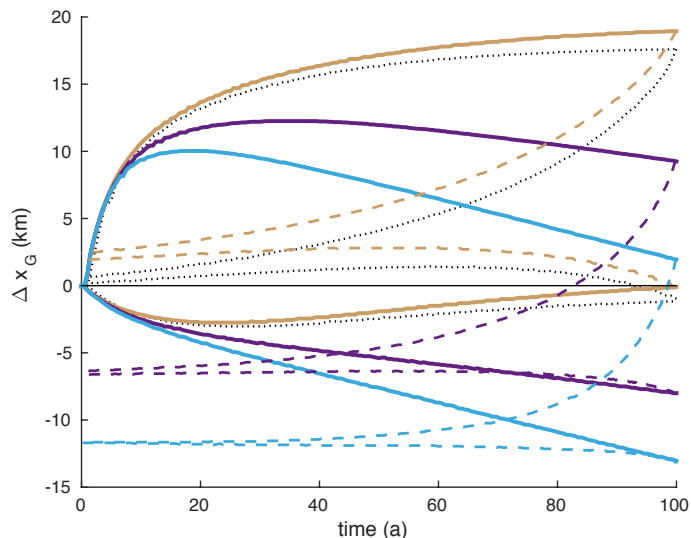


Figure 6. Experiment MISMIP3d P75S and P75R: time-dependent plot of the GL position relative to the steady position x_{G_0} (see Table 2) during (P75S; continuous) and after (P75R; dashed) the basal sliding perturbation, on the symmetry axis ($y = 0$; top curves) and on the free-slip boundary ($y = 50$ km; bottom curves) for the three different methods: LG (brown), DI (purple) and FF (blue). The black dotted curve is the GL evolution for the LFA solution published in Patyn et al. (2013) (LG method and $N_y = 20$). The mesh resolution in the y direction is $N_y = 20$ elements for all simulations.

Title Page

Abstract

Introduction

Conclusions

References

Tables

Figures

I ◀

▶ I

◀

▶

Back

Close

Full Screen / Esc

Printer-friendly Version

Interactive Discussion



Friction at GL in
Elmer/Ice

O. Gagliardini et al.

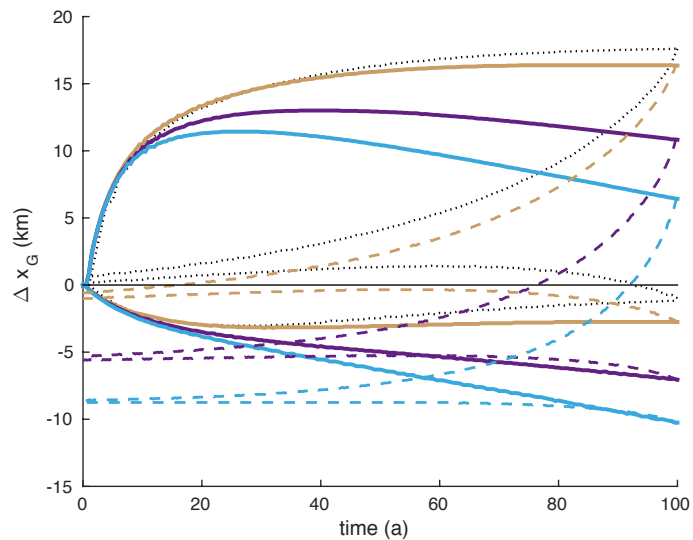


Figure 7. Same as Fig. 6 but for a lateral discretisation of $N_y = 40$ elements.

[Title Page](#)[Abstract](#)[Introduction](#)[Conclusions](#)[References](#)[Tables](#)[Figures](#)[◀](#)[▶](#)[◀](#)[▶](#)[Back](#)[Close](#)[Full Screen / Esc](#)[Printer-friendly Version](#)[Interactive Discussion](#)

Friction at GL in
Elmer/Ice

O. Gagliardini et al.

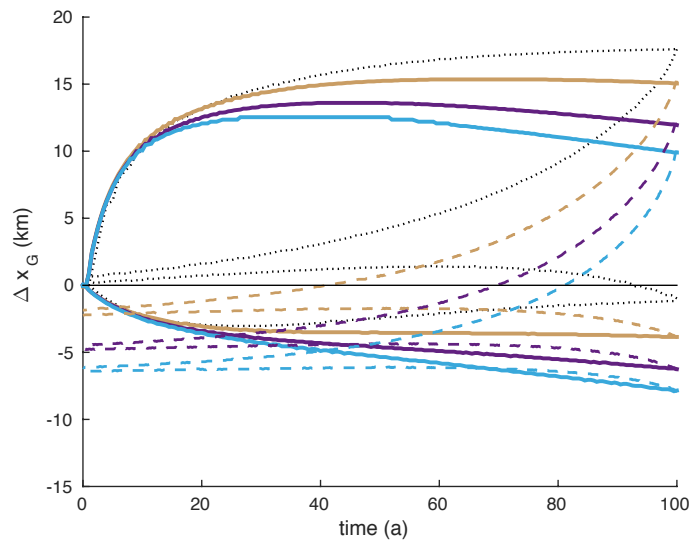


Figure 8. Same as Fig. 6 but for a lateral discretisation of $N_y = 80$ elements.

[Title Page](#)[Abstract](#)[Introduction](#)[Conclusions](#)[References](#)[Tables](#)[Figures](#)[◀](#)[▶](#)[◀](#)[▶](#)[Back](#)[Close](#)[Full Screen / Esc](#)[Printer-friendly Version](#)[Interactive Discussion](#)